direction. We applied light pulses to a ventricular region close to the bulbus to rhythmically activate ChR2 and found that cardiac conduction could be reversed (movie S11 and fig. S6) for at least 30 consecutive heartbeats.

Our results show that a surprisingly small number of pacemaker cells is indispensable for heartbeat initiation. This makes the embryonic heart very vulnerable, as no compensating mechanism seems to be in place on the time scales observed. Moreover, we have shown that this area can be optically targeted; our photostimulation methods allowed us to optically control heart rate, reverse cardiac conduction, and induce disease-like states in a reversible manner. This work opens a new avenue for controlling hemodynamic forces during studies on epigenetic factors of heart formation (*28*) and blood vessel development (*29*).

References and Notes

1. T. Mikawa, R. Hurtado, *Semin. Cell Dev. Biol.* **18**, 90 (2007).
2. M. R. Jongbloed, E. A. Mahtab, N. A. Blom, M. J. Schalij, A. C. Gittenberger-de Groot, *ScientificWorldJournal* **8**, 239 (2008).
3. K. Kamino, A. Hirota, S. Fujii, *Nature* **290**, 595 (1981).
4. D. Sedmera *et al.*, *Am. J. Physiol. Heart Circ. Physiol.* **284**, H1152 (2003).
5. N. C. Chi *et al.*, *PLoS Biol.* **6**, e109 (2008).
6. F. Zhang *et al.*, *Nature* **446**, 633 (2007).
7. M. Scanziani, M. Häusser, *Nature* **461**, 930 (2009).
8. L. Luo, E. M. Callaway, K. Svoboda, *Neuron* **57**, 634 (2008).
9. A. D. Douglass, S. Kraves, K. Deisseroth, A. F. Schier, F. Engert, *Curr. Biol.* **18**, 1133 (2008).
10. S. Szobota *et al.*, *Neuron* **54**, 535 (2007).
11. C. Wyart *et al.*, *Nature* **461**, 407 (2009).
12. H. Baier, E. K. Scott, *Curr. Opin. Neurobiol.* **19**, 553 (2009).
13. A. B. Arrenberg, F. Del Bene, H. Baier, *Proc. Natl. Acad. Sci. U.S.A.* **106**, 17968 (2009).
14. G. Nagel *et al.*, *Proc. Natl. Acad. Sci. U.S.A.* **100**, 13940 (2003).
15. E. K. Scott *et al.*, *Nat. Methods* **4**, 323 (2007).
16. O. G. Ayling, T. C. Harrison, J. D. Boyd, A. Goroshkov, T. H. Murphy, *Nat. Methods* **6**, 219 (2009).
17. J. Huisken, J. Swoger, F. Del Bene, J. Wittbrodt, E. H. Stelzer, *Science* **305**, 1007 (2004).
18. P. J. Scherz, J. Huisken, P. Sahai-Hernandez, D. Y. Stainier, *Development* **135**, 1179 (2008).
19. J. Huisken, D. Y. Stainier, *Opt. Lett.* **32**, 2608 (2007).
20. A. J. Sehnert *et al.*, *Nat. Genet.* **31**, 106 (2002).
21. R. Wilders, *Conf. Proc. IEEE Eng. Med. Biol. Soc.* **2007**, 152 (2007).
22. A. Nygren *et al.*, *Circ. Res.* **82**, 63 (1998).
23. See supporting material on *Science* Online.
24. D. Beis *et al.*, *Development* **132**, 4193 (2005).
25. D. Scherf, *Z. Gesamte Exp. Med.* **57**, 188 (1927).
26. M. W. Jenkins *et al.*, *Nat. Photonics* **4**, 623 (2010).
27. D. J. Milan, A. C. Giokas, F. C. Serluca, R. T. Peterson, C. A. MacRae, *Development* **133**, 1125 (2006).
28. J. R. Hove *et al.*, *Nature* **421**, 172 (2003).
29. C. Hahn, M. A. Schwartz, *Nat. Rev. Mol. Cell Biol.* **10**, 53 (2009).

30. We thank T. Mikawa, R. Shaw, and A. Müssigbrodt for feedback and comments on the manuscript. Supported by NIH grant HL54737 (D.Y.R.S.), the Packard Foundation (D.Y.R.S.), NIH grant R01 NS053358 (H.B.), a Sandler Opportunity Award, the Byers Award for Basic Science (H.B.), and the NIH Nanomedicine Development Center "Optical Control of Biological Functions" (H.B.). J.H. was supported by a Human Frontier Science Program (HFSP) cross-disciplinary fellowship. A.B.A. was supported by a Boehringer Ingelheim Fonds (B.I.F.) and a Krevans fellowship. The optogenetic idea, transgenic lines, and original observation originated in H.B.'s lab; follow-up experiments were carried out in D.Y.R.S.'s lab as an equal collaboration between A.B.A. and J.H. All authors worked on the manuscript, which was drafted by A.B.A. and J.H.

Supporting Online Material

www.sciencemag.org/cgi/content/full/330/6006/971/DC1
Materials and Methods
Figs. S1 to S7
Movies S1 to S11

2 August 2010; accepted 1 October 2010
10.1126/science.1195929

Kinetic Scaffolding Mediated by a Phospholipase C–β and G_q Signaling Complex

Gary L. Waldo,[1] Tiffany K. Ricks,[1] Stephanie N. Hicks,[1] Matthew L. Cheever,[1] Takeharu Kawano,[2] Kazuhito Tsuboi,[2] Xiaoyue Wang,[3] Craig Montell,[3] Tohru Kozasa,[2,4] John Sondek,[1,5,6] T. Kendall Harden[1,6]*

Transmembrane signals initiated by a broad range of extracellular stimuli converge on nodes that regulate phospholipase C (PLC)–dependent inositol lipid hydrolysis for signal propagation. We describe how heterotrimeric guanine nucleotide–binding proteins (G proteins) activate PLC-βs and in turn are deactivated by these downstream effectors. The 2.7-angstrom structure of PLC-β3 bound to activated $G\alpha_q$ reveals a conserved module found within PLC-βs and other effectors optimized for rapid engagement of activated G proteins. The active site of PLC-β3 in the complex is occluded by an intramolecular plug that is likely removed upon G protein–dependent anchoring and orientation of the lipase at membrane surfaces. A second domain of PLC-β3 subsequently accelerates guanosine triphosphate hydrolysis by $G\alpha_q$, causing the complex to dissociate and terminate signal propagation. Mutations within this domain dramatically delay signal termination in vitro and in vivo. Consequently, this work suggests a dynamic catch-and-release mechanism used to sharpen spatiotemporal signals mediated by diverse sensory inputs.

Phospholipase C (PLC) catalyzes the hydrolysis of phosphatidylinositol 4,5-bisphosphate [PtdIns(4,5)P_2] to the second messengers inositol 1,4,5-trisphosphate [Ins(1,4,5)P_3] and diacylglycerol in an essential step for the physiological action of many hormones, neurotransmitters, growth factors, and other extracellular stimuli (*1*–*3*). These cascades use signaling complexes consisting of Gα subunits of the G_q family ($G\alpha_q$, 11, 14, and 16) of heterotrimeric guanine nucleotide–binding proteins (G proteins) and PLC-β isozymes (β1-4) (*4*–*6*). Agonist-stimulated receptors increase exchange of guanosine triphosphate (GTP) for guanosine diphosphate (GDP) on $G\alpha_q$, GTP-bound $G\alpha_q$ engages and activates PLC-β, and PLC-β increases up to three orders of magnitude the rate of hydrolysis of GTP by its activating G protein (*7*–*9*). Coordination from upstream and downstream inputs sharpens time frame, amplitude, and on-off cycling of these signaling nodes. Although kinetic analyses revealed much about the dynamics of $G\alpha_q$/PLC-β signaling complexes (*10*–*12*), how PLC-βs simultaneously act as effectors and GTPase activating proteins (GAPs) has remained unknown. Here, we describe the structure of PLC-β3 in an activated complex with $G\alpha_q$, which together with supporting biochemical and physiological analyses reveals its mechanism of transmembrane signaling.

The three-dimensional structure of an AlF_4^--dependent complex of $G\alpha_q$ bound to PLC-β3 was solved by molecular replacement using PLC-β2 [Protein Data Bank (PDB) code 2FJU] and $G\alpha_q$ (PDB 2BCJ) as search models and refined at 2.7-Å resolution (table S1). PLC-β3 engages $G\alpha_q$ through three distinct regions (Fig. 1, A and B). First, an extended loop between the third and fourth EF hands of PLC-β3 directly buttresses switch residues critical for GTP hydrolysis by $G\alpha_q$. Second, the region of PLC-β3 that connects the catalytic TIM barrel and the C2 domain interacts with both switches 1 and 2 of $G\alpha_q$. Third, a segment composed of a helix-turn-helix at the C terminus of the C2 domain resides primarily within a shallow declivity on the surface of $G\alpha_q$ formed by switch 2 and α3. Other effectors are known to engage this region within Gα subunits (Fig. 1C). GTP hydrolysis by Gα subunits is independently accelerated by a large family of regulator of G protein signaling (RGS) proteins (*8*, *13*, *14*), and PLC-β3 interacts with a surface on $G\alpha_q$ that overlaps almost completely with portions of Gα subunits needed for engagement of RGS proteins (Fig. 1C). Consistent with a biologically relevant interface (*15*), the complex

[1]Department of Pharmacology, University of North Carolina School of Medicine, Chapel Hill, NC 27599, USA. [2]Department of Pharmacology, University of Illinois, Chicago, IL 60612, USA. [3]Departments of Biological Chemistry and Neuroscience, Center for Sensory Biology, Johns Hopkins University School of Medicine, Baltimore, MD 21205, USA. [4]Laboratory for Systems Biology and Medicine, Research Center for Advanced Science and Technology, University of Tokyo, Tokyo 153-8904, Japan. [5]Department of Biochemistry, University of North Carolina School of Medicine, Chapel Hill, NC 27599, USA. [6]Lineberger Cancer Center, University of North Carolina School of Medicine, Chapel Hill, NC 27599, USA.

*To whom correspondence should be addressed. E-mail: tkh@med.unc.edu

of PLC-β3 and $G\alpha_q$ buries ~3200 Å^2 of solvent-exposed surface area.

Activated $G\alpha_q$ does not impinge on the active site of PLC-β3 and indeed is at least 40 Å from the calcium ion cofactor needed for PtdIns(4,5)P_2 catalysis. Comparison of the structure of PLC-β3 in complex with $G\alpha_q$ to previous structures (*16*, *17*) of PLC-β2 indicates that lipase activation does not involve $G\alpha_q$-dependent propagation of a conformational change to the active site of the lipase (fig. S1A). Indeed, the active site of PLC-β3 is occluded by a portion of its X/Y linker (Fig. 1B): a poorly conserved loop that separates the two halves of the catalytic TIM barrel in all PLC isozymes. Our previous structural analyses illustrated that this region similarly occludes the active site of PLC-β2, and deletion of the negatively charged X/Y linker in PLC-β2, as well as in PLC-ε and -δ1, resulted in marked activation (*17*). Similarly, deletion of the highly negatively charged X/Y linker of PLC-β3 caused a large increase in lipase activity (fig. S1B), indicating that PLC-β3 also is robustly autoinhibited by its X/Y linker. Presumably, this region of PLC-β3 is forced out of the active site by steric and electrostatic repulsion mediated by the surface of the plasma membrane coupled to the engagement of $G\alpha_q$ (Fig. 1D). A similar mechanism was proposed previously for activation of PLC-β2 by Rac1, which binds entirely through the PH domain of PLC-β2 at substantial distance from the active site of the lipase (*16*). Consequently, $G\alpha_q$, Rac1, and likely other activators such as Gβγ activate PLC isozymes by anchoring and orienting them at substrate membranes to release autoinhibition by the X/Y linker and promote access of PtdIns(4,5)P_2 to the lipase active site.

PLC-β isozymes are effectors of $G\alpha_q$ as well as GAPs that enhance the intrinsic GTPase activity of the engaging Gα subunits. The structure of activated $G\alpha_q$ bound to PLC-β3 explains the integration of these reciprocal functions.

The catalytic core of the 13 mammalian PLC isozymes includes a pleckstrin homology (PH) domain, a set of four EF hands, a catalytic TIM barrel, and a C2 domain (*18*) (Fig. 1A). The canonical Gα effector-binding region of $G\alpha_q$, located between α3 and switch 2, is occupied by a helix-turn-helix (Hα1/Hα2) that immediately follows the C2 domain of PLC-β3 (Fig. 2A). PLC-δ isozymes terminate immediately after their C2 domain, which is the last common domain found in all PLC isozymes (*18*). Thus, grafting of Hα1/Hα2 onto the C terminus of the C2 domain of PLC-β3 provides a large binding surface that makes numerous contacts with $G\alpha_q$ (~1750 Å^2 of solvent accessible surface area buried). Only PLC-β isozymes are activated by $G\alpha_q$, and the highly conserved Hα1/Hα2 motif is found in all PLC-βs (Fig. 2B) but not in other PLC isozymes. PLC-βs also contain a long C-terminal region that extends about 300 residues past the Hα1/Hα2 module. This long C-terminal extension previously was thought to be important for interaction with $G\alpha_q$. However, absence of this region did not affect high affinity binding

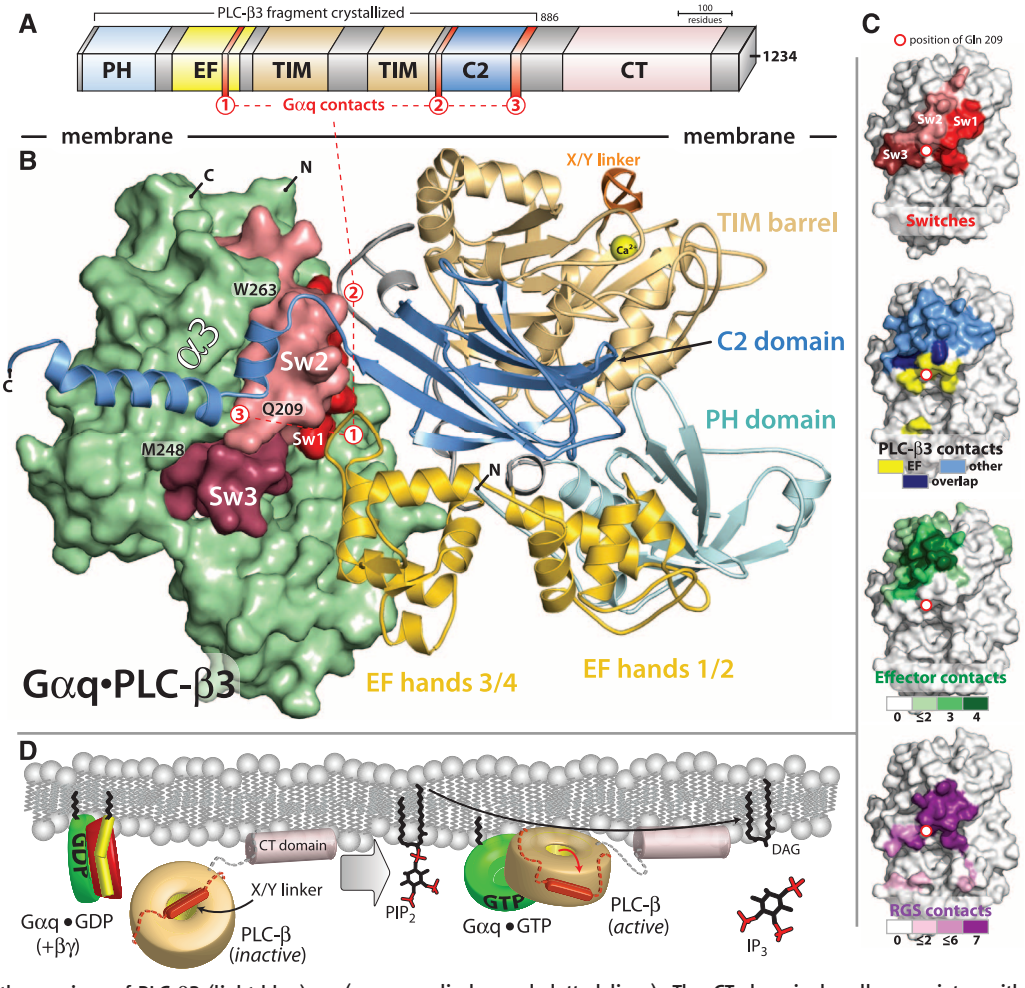

Fig. 1. Structure of $G\alpha_q$•PLC-β3. (**A**) Domain architecture of PLC-β3 drawn to scale and consisting of a N-terminal PH domain, a series of four EF hands, a catalytic TIM barrel, a C2 domain, and a carboxy-terminal (CT) domain. The CT domain is not necessary for $G\alpha_q$ binding (fig. S2), and, therefore, PLC-β3 truncated at residue 886 was used to facilitate crystallization. Three distinct regions of PLC-β3 that interact with G_q are indicated by red numerals. (**B**) Overall structure of the AlF_4^--dependent complex of $G\alpha_q$•PLC-β3 as viewed from the plane of the membrane. PLC-β3 is depicted as a ribbon cartoon with domains colored as in (A). Activated $G\alpha_q$ is depicted as a green surface with nucleotide-dependent switches (Sw1 to Sw3) in shades of red. Hα1/Hα2 (red 3) at the end of the C2 domain of PLC-β3 lies within the canonical effector-binding region of $G\alpha_q$ formed by α3 starting at M248 (*21*), the subsequent loop containing W263, and switch 2 containing Q209. The X/Y linker (orange) connects the two halves of the catalytic TIM barrel, and an ordered portion of the linker occludes the active site of the lipase highlighted by the Ca^{2+} (yellow ball) cofactor. (**C**) Surfaces of $G\alpha_q$ highlighting switches (top) in comparison to regions (lower images) of Gα subunits that interact with PLC-β3, other effectors, and RGS proteins. Interactions involving the EF3/4 loop are yellow except for overlap (dark blue) involving other regions of PLC-β3 (light blue). Gα subunits use a common interface (green) to engage four distinct effectors, and a different interface engages seven distinct RGS proteins (dark purple). Details of the analyses are supplied in (*41*). (**D**) Model for activation of PLC-β3 by GTP-activated $G\alpha_q$. $G\alpha_q$ (green) bound to GDP is sequestered by Gβγ (red and yellow) and does not interact with PLC-β, depicted as a gold toroid except for its CT domain (light pink) and X/Y linker (orange cylinder and dotted lines). The CT domain basally associates with membranes, whereas the X/Y linker blocks the lipase active site. Upon activation of heterotrimeric G_q, $G\alpha_q$-GTP dissociates from Gβγ and interacts with the main portion of PLC-β. Complex formation anchors and orients the lipase active site at membranes, leading to repulsion of the X/Y linker and freeing the active site for hydrolysis of PtdIns(4,5)P_2 into diacylglycerol (DAG) and Ins(1,4,5)P_3 (IP_3).

of PLC-β3 to $G\alpha_q$ [dissociation constant (K_d) ~ 200 nM; fig. S2], and it is not present in the PLC-β3 construct used for structure determination. The C-terminal domain is important for membrane association, but whether it has additional function(s) in the signaling complex remains unclear.

Pro^{862} of PLC-β3 lies within the turn between Hα1 and Hα2, makes extensive contacts with multiple residues of $G\alpha_q$, and forms the center of a $G\alpha_q$-binding interface (Fig. 2A). The side chain of the preceding Asn^{861} supports this turn by forming a hydrogen bond with the backbone amide of Lys^{864}. This Asn-Pro couplet is preserved in three of the four PLC-β isozymes (it is Asp-Pro in PLC-β4) and presumably defines the turn because of helix capping and breaking propensities of Asn/Asp and Pro, respectively. The turn is bracketed by Leu^{859}, which inserts into a hydrophobic pocket formed by residues in α3 and switch 2, and by Ile^{863}, which interacts with tandem glutamates in α3. Tyr^{855} in Hα1 and Asp^{870} in Hα2 also support the binding interface at the periphery. The binding of $G\alpha_q$ to Hα1/Hα2 of PLC-β3 recapitulates almost entirely the interaction of $G\alpha_q$ with several guanine nucleotide exchange factors (GEFs) for Rho, including p63RhoGEF, Trio, and Kalirin, which use a helix-turn-helix grafted onto the end of a DH/PH cassette to bind the α3/Sw2 declivity of $G\alpha_q$ (*19*, *20*) (Fig. 2C). PLC-β3 and p63RhoGEF use identical residues in their primary interfaces with $G\alpha_q$, and other effectors also engage this region of Gα subunits in similar fashion (Fig. 2C).

The role of Hα1/Hα2 residues in $G\alpha_q$-mediated activation was examined by mutational analyses. Whereas expression of $G\alpha_q$ or PLC-β3 alone in COS-7 cells had no effect, their coexpression resulted in a large increase in inositol lipid hydrolysis (fig. S3A). In contrast, coexpression of PLC-β3 with mutation $L^{859}\rightarrow E^{859}$ (*21*) [PLC-β3(L859E)] with $G\alpha_q$ had no effect over a broad range of conditions (fig. S3B). Gβγ independently activates PLC-β3, and coexpression of either PLC-β3 or PLC-β3(L859E) with $G\beta_1\gamma_2$ resulted in similar levels of activation (fig. S3C). Mutation of the analogous residue (Leu^{810}) in PLC-β1 also completely abrogated $G\alpha_q$-dependent stimulation (fig. S3D).

The contribution of residues across Hα1/Hα2 of PLC-β3 was examined (Fig. 2D and fig. S4). In each case, the relative sensitivity of the PLC-β3 mutant to activation by $G\alpha_q$ versus $G\beta_1\gamma_2$ was compared under conditions where maximal response to each activator was observed. Whereas single substitutions throughout Hα1/Hα2 did not affect Gβγ-stimulated activity (fig. S4), certain of these mutations (Y855A, L859A, N861A, P862A, and I863A) resulted in substantial or complete loss of the capacity of $G\alpha_q$ to promote PLC-β3–dependent increases in inositol phosphate accumulation (Fig. 2D).

The binding and lipase activities of PLC-β3 mutants also were tested by using purified proteins (fig. S5). PLC-β3, PLC-β3(L859E), and

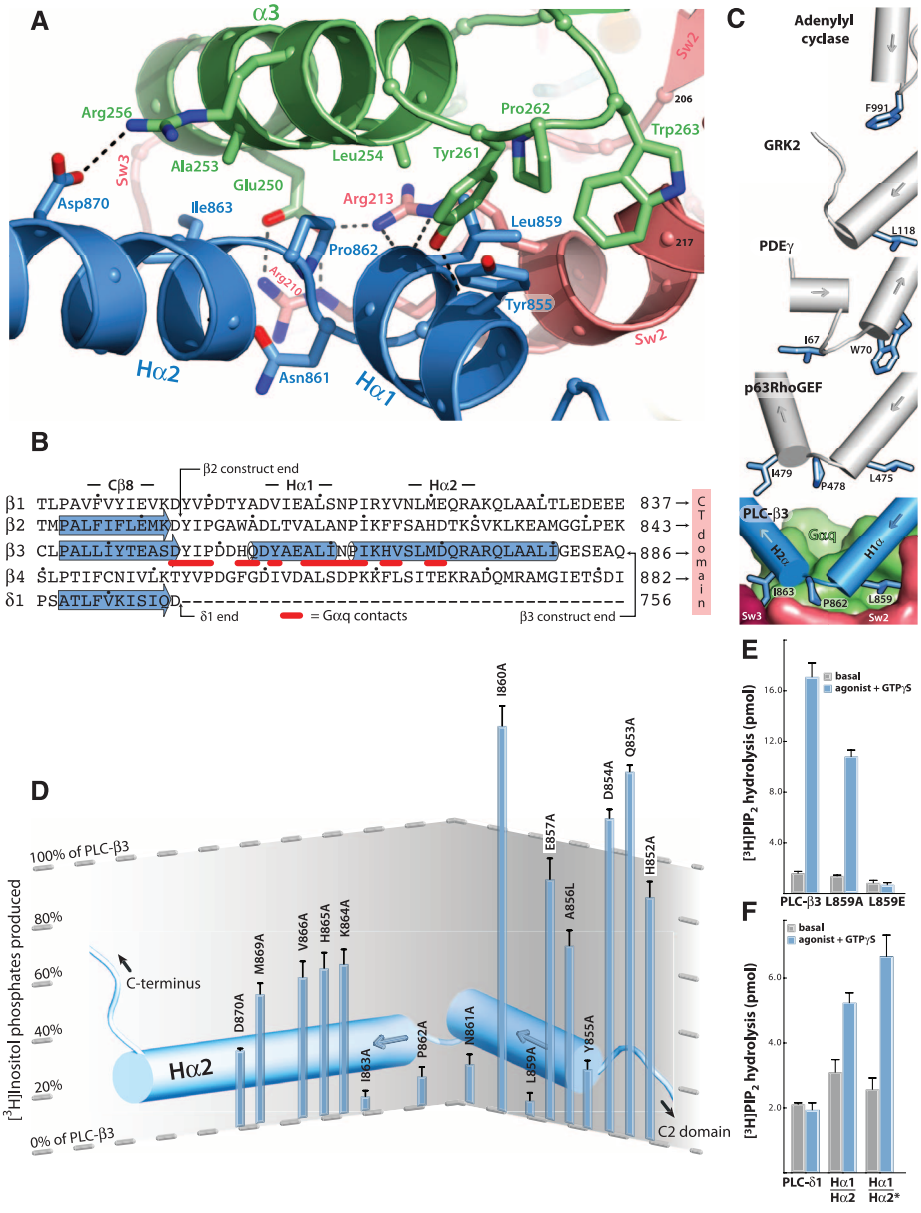

Fig. 2. Structure of the effector binding interface of $G\alpha_q$•PLC-β3. (**A**) Ribbon diagram of the interface between the Hα1/Hα2 region of PLC-β3 (blue) and the effector binding pocket of $G\alpha_q$ located between α3 (green) and Sw2 (pink). Interfacial residues (sticks) are labeled; hydrogen bonds are indicated by dashed lines. (**B**) Comparison of PLC sequences (*21*) at the end of the C2 domain (Cβ8) encompassing Hα1/Hα2. α helices (cylinders) and β sheets (arrows) were assigned by using crystal structures of PLC-β3 as reported here (PDB 3OHM), PLC-β2 (2ZKM), and PLC-δ1 (1DJX). C termini are indicated for full-length PLC-δ1 as well as the crystallized fragments of PLC-β2 and -β3. Residues in PLC-β3 that interact with $G\alpha_q$ are underlined in red. Dots indicate every 10th residue. (**C**) Comparison of effectors bound to Gα subunits. The major effector binding surface of $G\alpha_q$ (green with switches in red) engages Hα1/Hα2 (blue cylinders) of PLC-β3 through indicated residues (sticks) surrounding Pro^{862}. Structurally analogous α helices (gray cylinders) and residues (blue sticks) in other effectors are highlighted after superimposition of bound Gα subunits (not shown). PDE-γ, cyclic GMP phosphodiesterase-γ. (**D**) Mutational analyses of Hα1/Hα2. PLC-β3 mutants harboring the indicated single substitutions were assessed for capacity to be activated upon cotransfection with $G\alpha_q$ in COS-7 cells as measured by [^{3}H]inositol phosphate production. Further experimental details are described in figs. S3, A to C, and S4. (**E**) Requirement of Hα1/Hα2 for activation of PLC-β3 by $G\alpha_q$ assessed with purified proteins. [^{3}H]PtdIns(4,5)P_2-containing phospholipid vesicles reconstituted with purified $P2Y_1$ receptor, $G\alpha_q$, and $G\beta_1\gamma_2$ were used to assess the capacity of wild-type or PLC-β3 mutants (300 nM) to hydrolyze PtdIns(4,5)P_2 in the absence (basal) or presence of a $P2Y_1$ receptor agonist (2MeSADP, 1 μM) plus 100 nM GTPγS (agonist + GTPγS). Data are mean ± SEM from four independent experiments. (**F**) Grafting Hα1/Hα2 onto PLC-δ1 confers responsiveness to $G\alpha_q$. Activities of purified proteins were compared as in (E). Residues 847 to 886 of PLC-β3 were added to the end of PLC-δ1 to create PLC-δ1(Hα1/Hα2); starred variant consists of PLC-δ1(Hα1/Hα2) with additional substitutions (D610R and N612D) of PLC-δ1 to analogous PLC-β3 residues (see domain architectures in fig. S7A).

PLC-β3(L859A) exhibited similar basal lipase activities (fig. S5A) and were similarly activated by $Gβ_1γ_2$ (fig. S5B). However, the binding affinity of PLC-β3(L859A) for $Gα_q$ in the presence of AlF_4^- was sevenfold lower than PLC-β3, and no AlF_4^--dependent binding of PLC-β3(L859E) was observed (fig. S5C). Activities of PLC-β3 isozymes mutated in Hα1/Hα2 also differed markedly in a signaling complex reconstituted with purified $P2Y_1$ receptor, heterotrimeric G_q, and PLC-β3. The $P2Y_1$ receptor agonist, 2MeSADP, promoted robust activation of PLC-β3, but PLC-β3(L859E) was completely refractory to activation and intermediate activation was observed with PLC-β3(L859A) (Fig. 2E).

Alanine-scanning mutagenesis previously identified two small segments (residues 243 to 245 and 256 to 257) of $Gα_q$ necessary for elevated production of inositol phosphates (*22*). These regions contribute to interactions with Hα1/Hα2 (fig. S6A). Additional alanine substitutions were made in $Gα_q$, and, of those $Gα_q$ mutants that expressed as stable trypsin-resistant proteins, most exhibited a predictable loss in capacity to activate PLC-β3 (fig. S6B).

The loop between the end of the TIM barrel and the beginning of the C2 domain comprises a second distinct segment of PLC-β3 that makes extensive contacts with active $Gα_q$, including switches 1 and 2 (Fig. 3A). This interface includes a series of interdigitated pairs of charged residues, specifically (in PLC-β3/$Gα_q$) Asp^{709}/Arg^{202}, Lys^{710}/Glu^{191}, and Asp^{721}/Lys^{41}; these in turn are supported by additional charged residues (Glu^{703} and Arg^{707}) of PLC-β3. Alanine substitution of several of these residues in PLC-β3 compromised the capacity of $Gα_q$, but not $Gβ_1γ_2$, to activate PLC in COS-7 cells (Fig. 3B).

Residues adjacent to both borders of the C2 domain (Val^{724} and Tyr^{847}) converge to envelop His^{218} of $Gα_q$, which is wedged between the aforementioned interface and the start of Hα1/Hα2 to anchor two of the three major interfaces within the $Gα_q$•PLC-β3 complex (Fig. 3A). Mutation of His^{218} results in loss of capacity of $Gα_q$ to activate PLC-β3 (fig. S6B).

PLC-δ isozymes are not regulated by $Gα_q$, presumably because of lack of both Hα1/Hα2 and the $Gα_q$-interacting residues found in PLC-β isozymes between the TIM barrel and the C2 domain. Thus, we hypothesized that G protein–dependent regulation could be engineered into PLC-δ1 (fig. S7A). Surface plasmon resonance (SPR) analyses revealed that, whereas PLC-δ1 did not exhibit AlF_4^--dependent binding to $Gα_q$, introduction of the Hα1/Hα2 segment of PLC-β3 into PLC-δ1 conferred binding (fig. S7B). Moreover, receptor- and guanine nucleotide–stimulated lipase activity was observed with the chimeric isozymes but not PLC-δ1 (Fig. 2F), and the median effective concentration (EC_{50}) of GTPγS for activation of PLC-δ1(Hα1/Hα2) by GTPγS was 50 nM (fig. S7C). Thus, Hα1/Hα2 is a small, linear module used for functional engagement of $Gα_q$.

An extended loop between EF hands 3 and 4 of PLC-β3 interacts with the GTP-binding region of $Gα_q$ (Fig. 4A). This loop is highly conserved in all PLC-β isozymes, is not found in PLC-δ1 (Fig. 4B) or other PLC isozymes, and interacts with the active site of $Gα_q$. Asn^{260} of the EF3/4 loop promotes GTP hydrolysis by interaction with the side chain of Gln^{209} of $Gα_q$ (Fig. 4C), which rearranges during GTP hydrolysis to stabilize the transition state mimicked by GDP•AlF_4^-•H_20. Asn^{260} also interacts with Glu^{212} to stabilize switch 1 for GTP hydrolysis. The interactions of Asn^{260} of PLC-β3 with $Gα_q$ are recapitulated by a functionally equivalent asparagine in RGS9 (*23*) (Fig. 4C) and other RGS proteins (*24*, *25*).

Asn^{260} is positioned at the active site of $Gα_q$ as part of a tight turn (residue 260 to 264) of PLC-β3 that is stabilized by Glu^{261} and underpinned by an extensive series of hydrogen bonds principally mediated by Asp^{256} and Arg^{255} and Arg^{258} (Fig. 4A). These residues are highly conserved in all PLC-βs, as are Asn^{251} and Leu^{267}, which appear crucial in stabilizing the ends of the loop (Fig. 4B). The EF3/4 loop as well as other portions of EF hands 3 and 4 are disordered in the crystal structure of PLC-β2 (Fig. 4D). A likely scenario is that $Gα_q$ initially engages the EF3/4 loop of PLC-β3 to nucleate the underlying hydrogen bonding network and promote cooperative ordering of EF hands 3 and 4.

To directly examine the role of the EF3/4 region of PLC-β3 in mediating inactivation of its activating G protein, we quantified GTP hydrolysis by $Gα_q$ in the presence of purified PLC-β3 mutants (fig. S8A) by using phospholipid vesicles reconstituted with the $P2Y_1$ receptor and heterotrimeric G_q. In the presence of receptor agonist, PLC-β3 promoted up to 100-fold stimulation of GTP hydrolysis (Fig. 5A and fig. S8B), and activation occurred with an EC_{50} ~ 3 nM (table S2). A chimeric PLC-β3 replacing the EF3/4 loop with the analogous region of PLC-δ1 was severely crip-

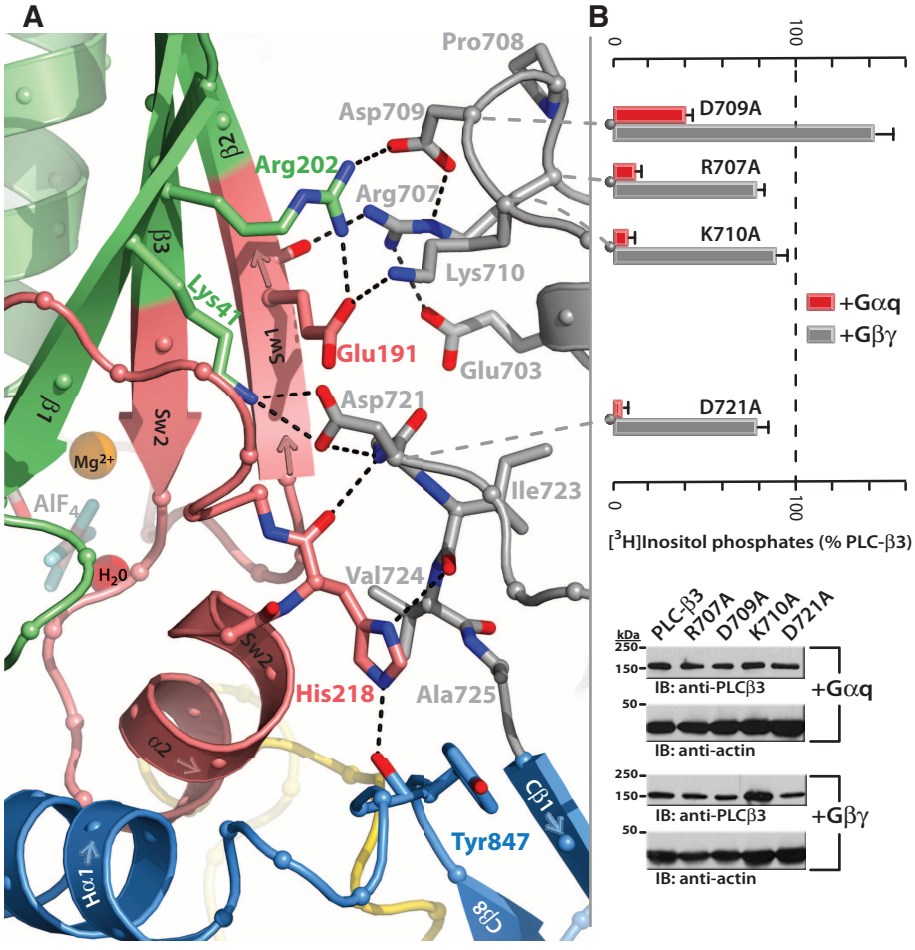

Fig. 3. Secondary $Gα_q$•PLC-β3 interface. (**A**) Ribbon diagram highlighting residues (gray) preceding the C2 domain (light blue) of PLC-β3 that interact with Sw1 and 2 (pink) of activated $Gα_q$ (green). AlF_4^- (gray cross-stick), Mg^{2+} (orange ball), and the catalytic water (red ball) within the nucleotide-binding pocket also are shown. (**B**) Mutational analysis of the $Gα_q$•PLC-β3 binding interface. (Top) Activation of the indicated mutants of PLC-β3 in the presence of cotransfected $Gα_q$ (red) or $Gβ_1γ_2$ (gray) was determined by quantification of [^{3}H]inositol phosphate accumulation in COS-7 cells. Data are mean ± SEM from four independent experiments. (Bottom) Relative expression of PLC-β3 and mutant forms was quantified under each transfection condition by using a PLC-β3–specific antibody. Actin immunoblots (IB) included as loading controls.

pled in its capacity to accelerate GTP hydrolysis by $G\alpha_q$ (Fig. 5A). Similarly, substitution of Asn^{260} dramatically reduced the capacity of PLC-β3 to promote GTP hydrolysis, whereas substitution of Val^{262} had negligible effect. Importantly, basal and Gβγ-stimulated lipase activities of these purified mutants were unaffected (fig. S8, A and C). The EC_{50} values of mutant and wild-type PLC-β3 for stimulation of GTP hydrolysis also were similar (table S2). In contrast, substitution of Leu^{859} to Ala^{859} within Hα1/Hα2, which reduced the binding affinity of the complex by ~sevenfold (fig S5C), also increased the EC_{50} for stimulation of GTP hydrolysis by ~10-fold (table S2). Thus, the EF3/4 loop of PLC-β3 is crucial for stimulation of GTP hydrolysis by $G\alpha_q$ but contributes minimally to forming the signaling complex.

Loss of capacity of PLC-β3 to promote GTP hydrolysis by $G\alpha_q$ should decrease its capacity to turn off subsequent to $G\alpha_q$-mediated activation. This idea was first tested in vitro with use of purified proteins. Addition of a $P2Y_1$ receptor antagonist (fig. S8, B and D) to an agonist preactivated signaling complex of the $P2Y_1$ receptor, heterotrimeric $G\alpha_q$, and wild-type PLC-β3 resulted in a rapid decline of lipase activity to levels similar to those observed in the absence of agonist (Fig. 5B). In contrast, little reversal of lipase activity occurred upon addition of $P2Y_1$ receptor antagonist to a similarly preactivated complex containing PLC-β3(δEF) (Fig. 5B).

Rhodopsin-initiated phototransduction in *Drosophila melanogaster* is mediated by $G\alpha_q$-dependent activation of PLC-β (*26*). To examine the role of the EF3/4 loop of PLC-β in a physiological system, we replaced wild-type PLC-β (NORPA) in *Drosophila* with a version mutated to alanine in the conserved Asn (N262) demonstrated above to be required for PLC-β-promoted GTP hydrolysis by $G\alpha_q$. Flies expressing wild-type NORPA or $NORPA^{N262A}$ exhibited similar amplitudes of the light-induced photoresponse (Fig. 5C). In contrast, whereas termination of light resulted in rapid termination of photoresponse in wild-type flies, we observed a marked defect in recovery with $norpA^{N262A}$.

PLC-β3 is a tumor suppressor, and its disruption in humans contributes to lymphomas and other myeloid malignancies (*27*, *28*). Similarly, $G\alpha_q$ is an oncogene, and its constitutive activation drives ~50% of all uveal melanomas (*29*). Signaling through the $G\alpha_q$/PLC-β axis is important for regulation of cell proliferation, and other disruptions in this node can be expected to contribute to cancer. In this regard, homozygous substitution of Arg^{254} within the EF3/4 loops of PLC-β4 was found in a pancreatic tumor during genome-wide profiling (*30*). The equivalent substitution in PLC-β3 resulted in a decrease in capacity to accelerate GTP hydrolysis by $G\alpha_q$ (Fig. 5D and fig. S8E).

The high-resolution structure of $G\alpha_q$•PLC-β highlights a dynamic interplay between regions of the complex needed to coordinate rapid activation and inactivation of this signaling node required for highly responsive, low-noise signal transduction. We propose that a conformationally flexible Hα1/Hα2 samples a relatively large volume to maximize probability of encounter-

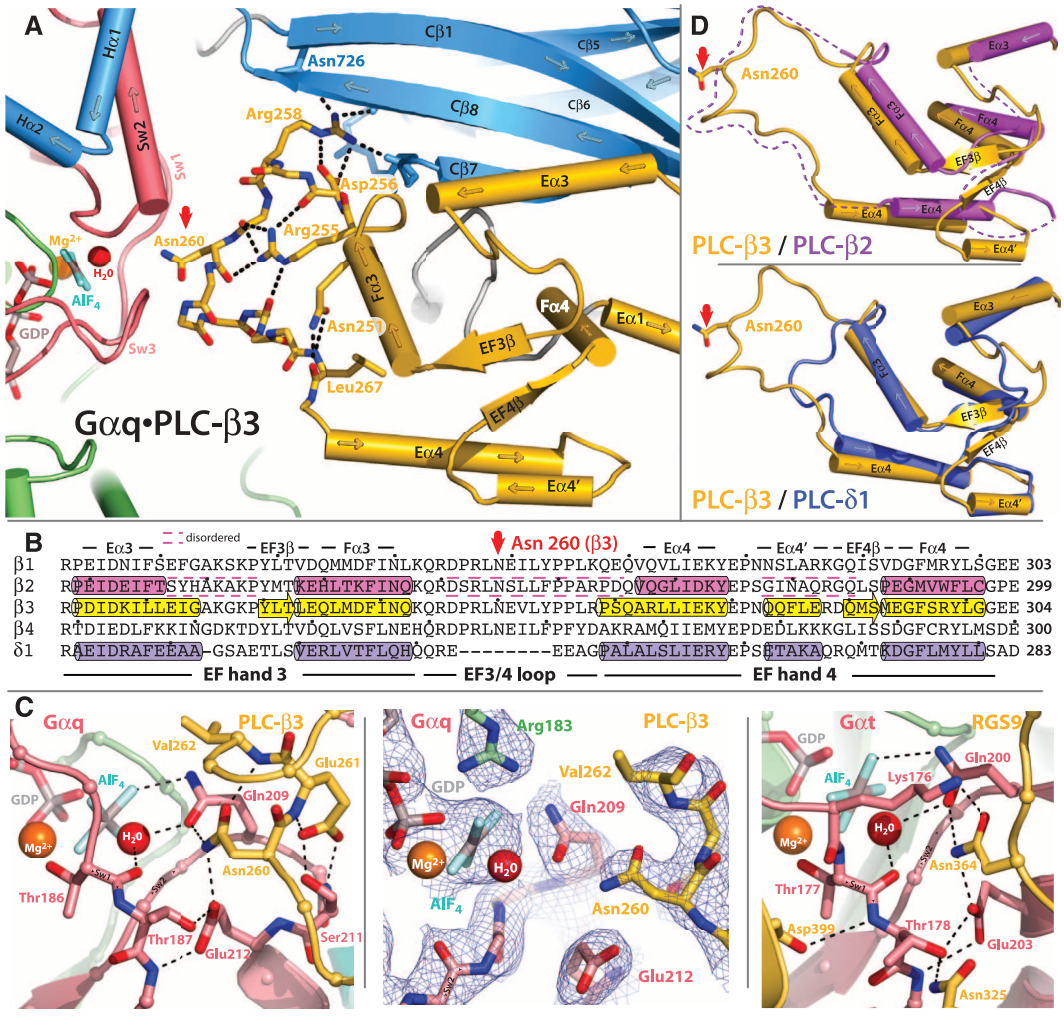

Fig. 4. Interaction of the EF3/4 loop of PLC-β3 with switch residues critical for GTP hydrolysis by $G\alpha_q$. (**A**) Ribbon and cylinder diagram highlighting conserved interactions within EF hands 3 and 4 (yellow) of PLC-β3 needed for the optimal positioning of Asn^{260} (red arrow) within the guanine nucleotide binding pocket of $G\alpha_q$. Sw1 to Sw3 are pink; other portions of $G\alpha_q$ are green. The C2 domain and adjacent Hα1/Hα2 of PLC-β3 are light blue; key PLC-β3 residues (sticks) and hydrogen bonds (dotted lines) that support Asn^{260} (red arrow) are highlighted. The guanine nucleotide binding pocket contains GDP and AlF_4^- (sticks) as well as the Mg^{2+} cofactor (orange ball) and catalytic water (red ball). (**B**) Sequence alignment comparing EF hands 3 and 4 of PLC-βs with equivalent region of PLC-δ1. α helices (cylinders) and β sheets (arrows) assigned from crystal structures (PLC-β3, 3OHM; PLC-β2, 2ZKM; δ1, 1DJX); dashed lines bracket disordered regions. The asparagine (Asn^{260} in PLC-β3) that is positioned for promotion of GTP hydrolysis by $G\alpha_q$ is indicated by a red arrow. The colors correspond to those of the structures depicted in (D) below. Dots indicate every 10th residue. (**C**) Comparison of the GTP-binding sites of $G\alpha_q$•PLC-β3 and $G\alpha_t$•RGS9. Left image depicts portions of the EF3/4 loop (yellow) of PLC-β3 contacting Sw1 and 2 (light red) of $G\alpha_q$. Other portions of $G\alpha_q$ are shown as in (A). Middle image highlights electron density (composite simulated annealing omit map contoured at 1.2 σ) centered on Asn^{260} of $G\alpha_q$•PLC-β3. Right image depicts analogous portions of RGS9 (yellow) bound to $G\alpha_t$ as revealed in the crystal structure determined by Slep *et al.* (*23*). (**D**) Ribbon and cylinder diagrams comparing EF hands 3 and 4 of PLC-β3 (yellow) with PLC-β2 (top, magenta) and PLC-δ1 (bottom, purple). Asn^{260} highlighted with red arrow, and dotted lines indicate disordered portions of PLC-β2.

ing $G\alpha_q$, and transient interactions with $G\alpha_q$ guide the final folding of Hα1/Hα2. The process of coupling folding with binding to increase the rate of formation of the final encounter complex has been described for other protein complexes (*31*, *32*) and is referred to as fly-casting. A subset of Dbl-family RhoGEFs typified by p63RhoGEF also apparently use fly-casting to engage $G\alpha_q$ (*19*, *20*). In particular, p63RhoGEF uses a helix-turn-helix immediately adjacent to a conserved PH domain to engage G_q in a fashion that is recapitulated almost identically in $G\alpha_q$•PLC-β. Thus, an independent module is grafted onto PLC-βs and RhoGEFs to confer binding to $G\alpha_q$. The Hα1/Hα2 module in PLC-βs is encoded by a single exon, which suggests that these signaling proteins acquired capacity to bind $G\alpha_q$ through intergenic exon shuffling.

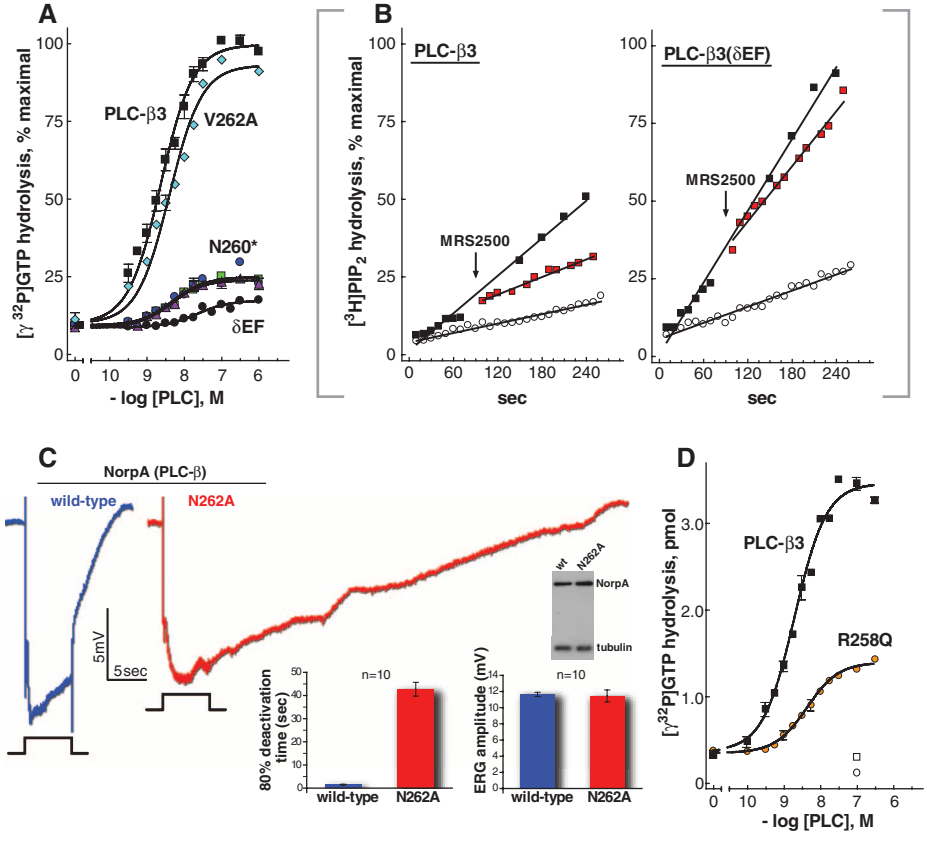

Fig. 5. Contribution of the EF hand region to GAP activity of PLC-β3. (**A**) The GAP activity of purified wild-type PLC-β3 is compared with that of mutant PLC-β3 isozymes. Steady-state GTP hydrolysis was quantified with phospholipid vesicles reconstituted with purified $P2Y_1$ receptor, $G\alpha_q$, and $G\beta_1\gamma_2$. Assays were in the presence of the $P2Y_1$ receptor agonist 2MeSADP (3 μM) and the indicated concentrations of purified PLC-β3; PLC-β3(δEF); PLC-β3(V262A); or PLC-β3(N260A), PLC-β3(N260G), or PLC-β3(N260S) [all designated as PLC-β3(N260*)] as described in (*41*). Data are plotted as percent of maximal response obtained with PLC-β3. Data are mean ± SEM of three experiments. (**B**) Deficiency in termination of $G\alpha_q$-stimulated PLC activity of a GAP-deficient mutant of PLC-β3. PLC activity was quantified with $[^3H]$PtdIns(4,5)P_2-containing phospholipid vesicles reconstituted with purified $P2Y_1$ receptor, $G\alpha_q$, and $G\beta_1\gamma_2$. Vesicles were incubated with 300 nM PLC-β3 or PLC-β3(δEF) in the absence (open circles) or presence of the $P2Y_1$ receptor agonist 2MeSADP (300 nM; black squares) and either 30 μM GTP or 100 nM GTPγS for 90 s before addition of $P2Y_1$ receptor antagonist MRS2500 (50 μM; red squares) or vehicle. Incubations were continued for an additional 165 s. Data are plotted as percent of the maximal response observed with either PLC-β3 or PLC-β3(δEF) in the presence of agonist plus GTPγS. (**C**) Delayed termination of the photoresponse in *Drosophila* expressing a GAP-deficient mutant of PLC-β. Electroretinograms from flies harboring wild-type PLC-β (NORPA, blue) or a mutant form ($NORPA^{N262A}$, red) deficient in capacity to accelerate the GTPase activity of $G\alpha_q$. Flies ~1 day posteclosion were dark-adapted for 2 min before exposure to 5-s pulses of orange light indicated by the event marker below each electroretinogram. At right are plotted deactivation rates and maximal amplitudes for the average of ten individual electroretinograms. Error bars indicate SEM. Expression of the *norpA* transgenes was confirmed by immunoblot (gel) of head extracts prepared from flies ~1 day posteclosion. (**D**) GAP activity of a mutant of PLC-β found in pancreatic cancer. PLC-β3 was mutated at a position (R258) (*21*) equivalent to a homozygous substitution identified in PLC-β4 during genome-wide profiling of pancreatic cancers (*30*). GAP activity of PLC-β3(R258Q) was compared with that of PLC-β3 as described in (A) above. Data are mean ± SEM of three experiments.

Engagement of PLC-β by $G\alpha_q$ is intimately coupled to inactivation of the complex. A primordial PLC-δ acquired an extended loop between EF hands 3 and 4 (Fig. 4D) that directly engages the switch regions of $G\alpha_q$ to stabilize the transition state for GTP hydrolysis. This EF3/4 loop and Hα1/Hα2 are linked evolutionarily, because both motifs are found in the two PLC-β isozymes of *Caenorhabditis elegans*. Indeed, they are not found separately in any PLC-β and therefore are the defining motifs of members of the PLC-β family. Taken together, we propose that $G\alpha_q$ is "caught" by a flycast from Hα1/Hα2 and is "released" by EF3/4 loop-mediated stimulation of GTP hydrolysis, which results in a conformational change in Sw2 and abrogation of the binding sites for both the EF3/4 loop and the Hα1/Hα2 segment. We also note that p115RhoGEF binds to $G\alpha_{13}$ and promotes GTP hydrolysis through two different domains (*33*).

Rapid cycling of effector engagement and GTP hydrolysis favors the maintenance of heterotrimeric G_q/effector complexes necessary for signal acuity in a process generally referred to as kinetic scaffolding (*9*, *10*, *34*, *35*). Phototransduction requires high signal amplification in rapid cycles of activation/deactivation in a signaling system organized for suppression of noise and therefore provides an excellent model for comparison of signaling mediated by PLC-βs and other effectors. Although $G\alpha_q$-promoted activation of PLC-β mediates phototransduction in some metazoans such as fruit flies, mammalian rod and cone phototransduction involves $G\alpha_t$-mediated activation of cyclic guanosine monophosphate (GMP) phosphodiesterase (PDE) (*36*). This PDE is not a GAP, and acceleration of GTP hydrolysis evolved in a separate protein, RGS9, which nonetheless stabilizes the switch regions of $G\alpha_t$ in much the way the EF3/4 loop of PLC-β stabilizes $G\alpha_q$ (*23*) (Fig. 4C). The binding of PDE to the effector pocket of $G\alpha_t$ allosterically increases binding of RGS9 (*23*, *37*). G protein–coupled receptor kinase 2 (GRK2) and, to a lesser extent, p63RhoGEF enhance the GAP activity of RGS4 in a complex with $G\alpha_q$ (*38*). This allostery is inherent in the catch-and-release mechanism used by PLC-βs. Ablation of GAP function of PLC-β markedly prolongs deactivation of phototransduction in *Drosophila* (Fig. 5C), and disruption of RGS9 in mice (*39*) and mutation of RGS9 in human disease (*40*) produce analogous phenotypes.

References and Notes

1. M. J. Berridge, R. F. Irvine, *Nature* **312**, 315 (1984).
2. R. H. Michell, *Biochim. Biophys. Acta* **415**, 81 (1975).
3. Y. Nishizuka, *Science* **258**, 607 (1992).
4. A. V. Smrcka, J. R. Hepler, K. O. Brown, P. C. Sternweis, *Science* **251**, 804 (1991).
5. S. J. Taylor, H. Z. Chae, S. G. Rhee, J. H. Exton, *Nature* **350**, 516 (1991).
6. G. L. Waldo, J. L. Boyer, A. J. Morris, T. K. Harden, *J. Biol. Chem.* **266**, 14217 (1991).
7. W. D. Singer, H. A. Brown, P. C. Sternweis, *Annu. Rev. Biochem.* **66**, 475 (1997).
8. E. M. Ross, T. M. Wilkie, *Annu. Rev. Biochem.* **69**, 795 (2000).
9. E. M. Ross, *Curr. Biol.* **18**, R777 (2008).

10. G. H. Biddlecome, G. Berstein, E. M. Ross, *J. Biol. Chem.* **271**, 7999 (1996).
11. S. Mukhopadhyay, E. M. Ross, *Proc. Natl. Acad. Sci. U.S.A.* **96**, 9539 (1999).
12. M. Turcotte, W. Tang, E. M. Ross, *PLoS Comput. Biol.* **4**, e1000148 (2008).
13. R. R. Neubig, D. P. Siderovski, *Nat. Rev. Drug Discov.* **1**, 187 (2002).
14. H. G. Dohlman, J. Thorner, *J. Biol. Chem.* **272**, 3871 (1997).
15. P. Chakrabarti, J. Janin, *Proteins* **47**, 334 (2002).
16. M. R. Jezyk *et al.*, *Nat. Struct. Mol. Biol.* **13**, 1135 (2006).
17. S. N. Hicks *et al.*, *Mol. Cell* **31**, 383 (2008).
18. T. K. Harden, J. Sondek, *Annu. Rev. Pharmacol. Toxicol.* **46**, 355 (2006).
19. R. J. Rojas *et al.*, *J. Biol. Chem.* **282**, 29201 (2007).
20. S. Lutz *et al.*, *Science* **318**, 1923 (2007).
21. Single-letter abbreviations for the amino acid residues are as follows: A, Ala; C, Cys; D, Asp; E, Glu; F, Phe; G, Gly; H, His; I, Ile; K, Lys; L, Leu; M, Met; N, Asn; P, Pro; Q, Gln; R, Arg; S, Ser; T, Thr; V, Val; W, Trp; and Y, Tyr.
22. G. Venkatakrishnan, J. H. Exton, *J. Biol. Chem.* **271**, 5066 (1996).
23. K. C. Slep *et al.*, *Nature* **409**, 1071 (2001).
24. K. C. Slep *et al.*, *Proc. Natl. Acad. Sci. U.S.A.* **105**, 6243 (2008).
25. J. J. G. Tesmer, D. M. Berman, A. G. Gilman, S. R. Sprang, *Cell* **89**, 251 (1997).
26. T. Wang, C. Montell, *Pfugers Arch.* **454**, 821 (2007).
27. C. G. Mullighan *et al.*, *Nature* **446**, 758 (2007).
28. W. Xiao *et al.*, *Cancer Cell* **16**, 161 (2009).
29. C. D. Van Raamsdonk *et al.*, *Nature* **457**, 599 (2009).
30. S. Jones *et al.*, *Science* **321**, 1801 (2008); 10.1126/science.1164368.
31. B. A. Shoemaker, J. J. Portman, P. G. Wolynes, *Proc. Natl. Acad. Sci. U.S.A.* **97**, 8868 (2000).
32. K. Sugase, H. J. Dyson, P. E. Wright, *Nature* **447**, 1021 (2007).
33. Z. Chen, W. D. Singer, P. C. Sternweis, S. R. Sprang, *Nat. Struct. Mol. Biol.* **12**, 191 (2005).
34. C. A. Doupnik, N. Davidson, H. A. Lester, P. Kofuji, *Proc. Natl. Acad. Sci. U.S.A.* **94**, 10461 (1997).
35. H. Zhong *et al.*, *J. Biol. Chem.* **278**, 7278 (2003).
36. V. Y. Arshavsky, T. D. Lamb, E. N. Pugh Jr., *Annu. Rev. Physiol.* **64**, 153 (2002).
37. N. P. Skiba, J. A. Hopp, V. Y. Arshavsky, *J. Biol. Chem.* **275**, 32716 (2000).
38. A. Shankaranarayanan *et al.*, *J. Biol. Chem.* **283**, 34923 (2008).
39. C. K. Chen *et al.*, *Nature* **403**, 557 (2000).
40. K. M. Nishiguchi *et al.*, *Nature* **427**, 75 (2004).
41. Materials and methods are available as supporting material on *Science* Online.
42. This research was supported by NIH grants GM38213 and GM57391 (J.S. and T.K.H.), GM61454 and GM074001 (T.K.), and EY010852 (C.M.). T.K.R. was supported by a Ruth L. Kirschstein National Service Award F31 Predoctoral Fellowship and a United Negro College Fund Merck Graduate Science Research Dissertation Fellowship. K.T. was supported by a Postdoctoral Fellowship for Research Abroad from the Japan Society for the Promotion of Science. We acknowledge the outstanding help with structural analyses by B. Temple, L. Betts, J. Vanhooke, T. Charpentier, V. Arshavsky, and M. Kosloff; with analysis of linker-deleted PLC-β3 by N. Vincent Jordan; with SPR analyses by A. Kimple; with [γ^{32}P]GTP purification by E. Lazarowski and the insightful comments on the manuscript by H. Dohlman, R. Nicholas, E. Ross, and K. Slep. Coordinates and structure factors for $G\alpha_q$•PLC-β3 have been deposited under the PDB accession code 3OHM.

Supporting Online Material

www.sciencemag.org/cgi/content/full/science.1193438/DC1
Materials and Methods
SOM Text
Figs. S1 to S8
Tables S1 to S2
References

8 June 2010; accepted 14 September 2010
Published online 21 October 2010;
10.1126/science.1193438
Include this information when citing this paper.

Peripherally Applied Aβ-Containing Inoculates Induce Cerebral β-Amyloidosis

Yvonne S. Eisele,[1,2] Ulrike Obermüller,[1,2] Götz Heilbronner,[1,2,3] Frank Baumann,[1,2] Stephan A. Kaeser,[1,2] Hartwig Wolburg,[4] Lary C. Walker,[5] Matthias Staufenbiel,[6] Mathias Heikenwalder,[7] Mathias Jucker[1,2]*

The intracerebral injection of β-amyloid–containing brain extracts can induce cerebral β-amyloidosis and associated pathologies in susceptible hosts. We found that intraperitoneal inoculation with β-amyloid–rich extracts induced β-amyloidosis in the brains of β-amyloid precursor protein transgenic mice after prolonged incubation times.

Intracerebral inoculation with minute amounts of brain extract containing misfolded β-amyloid (Aβ) from patients with Alzheimer's disease or from amyloid-bearing β-amyloid precursor protein (APP) transgenic (tg) mice induces cerebral β-amyloidosis and related pathologies in APP tg mice in a time- and concentration-dependent manner (*1*). However, oral, intravenous, intraocular, or intranasal inoculations have failed to induce cerebral β-amyloidosis in APP tg hosts (*2*). These findings suggest that Aβ-containing brain material in direct contact with the brain can induce cerebral β-amyloidosis, but that, unlike prions, either the inducing agent is not readily conveyed from peripheral sites to the brain or a higher concentration or longer incubation period is required for peripherally delivered Aβ seeds.

Intraperitoneal administration of prion-rich material is more efficient at transmitting prion disease than is oral administration (*3*, *4*). To test whether intraperitoneal inoculation of Aβ-rich material might similarly trigger Aβ misfolding and deposition in the brain, we administered two intraperitoneal injections (100 μl each, 1 week apart) of Aβ-laden (10 to 20 ng/μl) brain extract from aged APP23 tg mice (Tg extract) to a cohort of young (2-month-old) female APP23 tg mice (*5*). After a 7-month incubation period, cerebral β-amyloidosis was robustly induced in all intraperitoneally inoculated mice compared with untreated littermate controls (Fig. 1). To confirm this finding, we inoculated a second cohort of 2-month-old female APP23 mice with a different batch of Tg brain extract in another laboratory (cohort 2, Tübingen, versus cohort 1, Basel). After 6 to 7 months, mice injected intraperitoneally with the Tg extract exhibited robust cerebral β-amyloidosis, whereas intraperitoneal inoculation with phosphate-buffered saline (PBS) or brain extract from age-matched, non-tg wild-type mice (Wt extract) was ineffective (Fig. 1).

Induced β-amyloidosis was strongest in the anterior and entorhinal cortices, with additional deposition in the hippocampus, resembling the regional development of endogenous β-amyloidosis in aged APP23 mice (*6*). However, whereas normal aged APP23 mice manifest mostly parenchymal deposits, the induced β-amyloid in intraperitoneally seeded mice was predominantly associated with blood vessels [cerebral β-amyloid angiopathy (Aβ-CAA)], often with massive spreading into the neighboring brain parenchyma (Fig. 1). The presence of Aβ was confirmed by immunoblotting, and amyloid fibrils were evident ultrastructurally; in addition, the induced β-amyloidosis was linked to gliosis, hyperphosphorylated tau, and other associated pathologies (Fig. 2), reminiscent of the cerebral β-amyloid deposition in aged APP23 mice (*6*, *7*).

To compare the efficiency and time course of intraperitoneal versus intracerebral inoculation, 2-month-old female APP23 mice were inoculated either intraperitoneally (2 × 100 μl) or intracerebrally (2.5 μl into the hippocampus) with Tg extract, and then analyzed 4 months later. No cerebral β-amyloid induction was found in any of the four intraperitoneally inoculated mice, whereas all six intracerebrally inoculated mice revealed β-amyloid induction identical to that previously reported (*1*, *2*). From this observation, together with previous time course and 1:20 dilution experiments for intracerebral inoculations (*1*), we estimate that intraperitoneal inoculations with 1000 times as much Aβ take 2 to 5 months longer to induce cerebral β-amyloidosis than do intracerebral inoculations.

The replication of peripherally applied prions and their translocation into the central nervous

[1]Department of Cellular Neurology, Hertie-Institute for Clinical Brain Research, University of Tübingen, D-72076 Tübingen, Germany. [2]DZNE–German Center for Neurodegenerative Diseases, D-72076 Tübingen, Germany. [3]Graduate School for Cellular and Molecular Neuroscience, University of Tübingen, D-72074 Tübingen, Germany. [4]Department of Pathology, University of Tübingen, D-72076 Tübingen, Germany. [5]Yerkes National Primate Research Center and Department of Neurology, Emory University, Atlanta, GA 30322, USA. [6]Novartis Institutes for Biomedical Research, Neuroscience Discovery, CH-4056 Basel, Switzerland. [7]Department of Pathology, Institute for Neuropathology, University Hospital, CH-8091 Zürich, Switzerland.

*To whom correspondence should be addressed. E-mail: mathias.jucker@uni-tuebingen.de

Kinetic Scaffolding Mediated by a Phospholipase C–β and G_q Signaling Complex

Gary L. Waldo, *et al.*

Science **330**, 974 (2010);
DOI: 10.1126/science.1193438